

TECHNICAL ADVANCE

Visualising the ionome in resistant and susceptible plant-pathogen interactions

Sophie M. Brouwer^{1,*}  Patric Lindqvist-Reis^{1,2}, Daniel P. Persson³, Salla Marttila¹, Laura J. Grenville-Briggs¹ and Erik Andreasson¹

¹Department of Plant Protection Biology, Swedish University of Agricultural Sciences, Alnarp, Sweden,

²Institute for Nuclear Waste Disposal, Karlsruhe Institute of Technology, Karlsruhe, Germany, and

³Department of Plant and environmental Sciences (PLEN), University of Copenhagen, Copenhagen, Denmark

Received 25 November 2020; revised 29 July 2021; accepted 9 August 2021; published online 18 August 2021.

*For correspondence (e-mail sophie.brouwer@slu.se).

SUMMARY

At the morphological and anatomical levels, the ionome, or the elemental composition of an organism, is an understudied area of plant biology. In particular, the ionomic responses of plant-pathogen interactions are scarcely described, and there are no studies on immune reactions. In this study we explored two X-ray fluorescence (XRF)-based ionome visualisation methods (benchtop- and synchrotron-based micro-XRF [μ XRF]), as well as the quantitative inductively coupled plasma optical emission spectroscopy (ICP-OES) method, to investigate the changes that occur in the ionome of compatible and incompatible plant-pathogen interactions. We utilised the agronomically important and comprehensively studied interaction between potato (*Solanum tuberosum*) and the late blight oomycete pathogen *Phytophthora infestans* as an example. We used one late blight-susceptible potato cultivar and two resistant transgenic plant lines (only differing from the susceptible cultivar in one or three resistance genes) both in control and *P. infestans*-inoculated conditions. In the lesions from the compatible interaction, we observed rearrangements of several elements, including a decrease of the mobile macronutrient potassium (K) and an increase in iron (Fe) and manganese (Mn), compared with the tissue outside the lesion. Interestingly, we observed distinctly different distribution patterns of accumulation at the site of inoculation in the resistant lines for calcium (Ca), magnesium (Mg), Mn and silicon (Si) compared to the susceptible cultivar. The results reveal different ionomes in diseased plants compared to resistant plants. Our results demonstrate a technical advance and pave the way for deeper studies of the plant-pathogen ionome in the future.

Keywords: ionome, lateblight, phytophthora, plantpathogen, potato, XRF, technical advance.

INTRODUCTION

The plant ionome, or chemical element composition, is dependent on the nutrients available in the soil. For agricultural crops, the available nutrients are often supplemented with fertilisers. To ensure optimal nutrient availability for plant growth and yield, the best fertiliser regimes have been well studied (Jenkins and Ali, 2000; Meyer-Aurich *et al.*, 2010; Prummel and Barnau-Sijthoff, 1984; Westermann, 2005; Yousaf *et al.*, 2017). However, optimal and crop-specific fertilisation can also be employed in disease control, since plant nutritional status also affects disease tolerance and resistance to pathogens (Dordas, 2008).

The relationship between plant nutrients and pathogenesis has mostly been studied in plants suffering from

various deficiencies (Graham and Webb, 2018). For example, Amtmann *et al.* (2008) combined field evidence and metabolic knowledge to provide an overview of the interaction between potassium (K) nutrition, diseases and pest incidences. They showed that deficiency in K results in loss of mechanical resistance, due to loss of cell wall rigidity. Additionally, they showed that K deficiency results in changes in the metabolic profile, such as an increase in sugars and amino acids, which potentially increases the attractiveness of a plant for pathogen infection. Thus, some nutrient deficiencies can increase the susceptibility of a plant to disease. On the other hand, some deficiencies can also lead to increased resistance to plant pathogens. For example, Kieu *et al.* (2012) showed that *Arabidopsis*

thaliana plants deficient in iron (Fe) were more resistant to the bacterium *Dickeya dadantii* and the fungus *Botrytis cinerea*. In plants with sufficient nutrient levels, however, little is known about how the re-allocation of nutrients and beneficial elements within the damaged tissue may contribute to pathogen resistance or susceptibility. De La Fuente *et al.* (2013) investigated the changes in the leaf ionome in tobacco (*Nicotiana tabacum*) upon infection with the bacterial pathogen *Xylella fastidiosa*, and Nicolas *et al.* (2019) studied ionomic changes in lettuce infected with the causal agent of bacterial leaf spot, *Xanthomonas campestris* pv. *vitians*. Both of these studies analysed the ionomes using inductively coupled Plasma optical emission spectroscopy (ICP-OES). De la Fuente *et al.* (2013) found that tobacco leaves infected with *X. fastidiosa* had a significantly increased calcium (Ca) content and a decreased phosphorus (P) content compared to uninfected plants, an observation that also held true for *X. fastidiosa*-infected leaf material from plants collected from the field. Nicolas *et al.* (2019) found several differences in the element composition between *X. campestris* pv. *vitians*-infected and uninfected lettuce. In this study, P decreased relative to nitrogen (N) and sulphur (S) in infected material, since the N-S ratio increases relative to the N-P ratio during infection, similar to the results from tobacco (De La Fuente *et al.*, 2013). No ionome study has been carried out at the morphological or anatomical level in this context or in relation to plant immunity.

Potato (*Solanum tuberosum*) is the third most important food crop for human consumption and has a great cultural significance (e.g., Eriksson *et al.*, 2016). However, the production of potato is plagued by multiple pathogens, leading to extensive use of chemical pesticides and fungicides. The most devastating pathogen for potato production worldwide is the oomycete *Phytophthora infestans*, the causal agent of late blight. The host plant defends itself against the disease by producing physical barriers and employing immune strategies, such as effector-triggered immunity (ETI). In the ETI response, resistance (R)-genes play a key role. The encoded R-proteins recognise, or contribute to the recognition of, pathogen-derived effectors. The detection and recognition of pathogen-derived effector proteins by R-proteins triggers multiple signal cascades and responses such as the hypersensitive response (HR) and the production of secondary metabolites and reactive oxygen species (ROS) (Jones and Dangl, 2006; Wang *et al.*, 2019). Several of these R-genes have been identified in wild relatives of potato and have subsequently been introduced into cultivated potato to confer resistance against late blight. For example, the R-genes *Rpi-blb1* and *Rpi-blb2* both come from the wild potato species *Solanum bulbocastanum*, and the R-gene *Rpi-vnt1.1* comes from the wild potato species *Solanum venturii* (Foster *et al.*, 2009; Song *et al.*, 2003; van der Vossen *et al.*, 2003, 2005).

Phytophthora infestans is notorious for being a highly adaptable pathogen that can rapidly overcome such single R-gene resistance (Fry, 2008). Hence, relying solely on single R-genes might not be durable, and therefore stacking of multiple R-genes is now being used (Ghislain *et al.*, 2019; Wang *et al.*, 2020; Zhu *et al.*, 2012). To ensure the optimal combination of R-genes for stacking in future breeding programmes, a greater understanding of resistant and susceptible reactions on multiple levels could potentially help the durability as well as aid the design of improved means of integrated disease management (IDM). One significant knowledge gap is ionome changes during plant-microbe interactions, the study of which has largely been technically limited until now.

To study the ionome, experimental methods capable of distinguishing chemical elements within a sample are required. Two such methods are X-ray fluorescence (XRF)- and ICP-based techniques. XRF methods are able to distinguish chemical elements since after excitation with high-energy X-rays, the atoms from each chemical element release fluorescence at characteristic energy levels (Salt *et al.*, 2008; Shackley, 2018). In ICP methods, the atoms in a sample are brought into an ionized state in the inductively heated plasma. Once the atoms fall back to the ground state, photons characteristic of each chemical element are emitted (Caruso *et al.*, 2017). For both methods a detector able to capture the fluorescence or photons is required to collect data. Thus, the chemical element composition, or ionome, of a sample can subsequently be determined (Caruso *et al.*, 2017; Salt *et al.*, 2008; Shackley, 2018).

In this study, we used XRF methods at two scales, a commercially available micro-XRF (μ XRF) benchtop machine and a synchrotron-based μ XRF imaging method, utilising specialised beamlines available at particle accelerators all over the world. We used these two methods to visualise the ionome changes after inoculation with *P. infestans* in a susceptible potato cultivar and two R-gene-expressing transgenic plant lines in the cultivar background, only differing from the cultivar in one or three R-genes. We also compared these visualisation methods to ICP-OES. Our data show that both XRF- and ICP-based methods are applicable to the study of ionomic changes that occur in plant-pathogen interactions, representing a significant technical advance in the research field.

RESULTS

Lesion development in the different plant lines

To visualise and compare the ionome responses of disease and immune reactions, we utilised three plant lines only differing in one or three R-genes: a commercially available potato cultivar (cv. *Désirée*), which is susceptible to *P. infestans*, and two transgenic plant lines, previously

created in our group, containing *Resistance to P. infestans* (*Rpi*) genes in the cv. Désirée background. One of the transgenic lines contains the *Rpi-blb1* resistance gene (Abreha *et al.*, 2015), and the other contains a stack of the three R-genes *Rpi-blb1*, *Rpi-blb2* and *Rpi-vnt1.1* (Wang *et al.*, 2020). Hereafter, the plant lines are referred to as cv. Désirée for the susceptible cultivar and 1R and 3R for the two transgenic lines. In response to inoculation with *P. infestans*, cv. Désirée developed large lesions with distinct infection zones (Figure 1b), whilst, as expected, the resistant plant lines did not develop any disease-related lesions upon infection with *P. infestans*. The 1R line developed distinct macroscopic HR lesions on and around the area where the inoculation droplet was placed (Figure 1b). These lesions were similar in size to previously described HR responses in plants expressing the same R-gene (*Rpi-blb1*) (Abreha *et al.*, 2015; Champouret *et al.*, 2009; van der Vossen *et al.*, 2003). The 3R line only developed small HR lesions that were macroscopically barely visible (Figure 1b), in agreement with results obtained for five independent transformation lines described in Wang *et al.* (2020).

Benchtop μXRF elemental maps reveal distribution of chemical elements

We used a benchtop μXRF spectrometer to obtain two-dimensional chemical element distribution maps of relatively large sections ($20 \times 20 \text{ mm}^2$) of potato leaves. We scanned both *P. infestans*-inoculated and mock-inoculated freeze-dried leaflets from all three plant lines. Chemical element distribution maps were obtained for nine different elements that were possible to measure using this experimental setup: the macronutrients P, K, S, Ca and magnesium (Mg) (Figure 2 and File S1) and the micronutrients and trace elements Fe, manganese (Mn), aluminium (Al) and silicon (Si) (Figure 3 and File S1). The pixel intensity scale in Figures 2 and 3 going from purple (low concentration) to white (high concentration) of the images are for visualisation of the element distribution within one image and should not be used for comparison between images. To compare the average chemical element composition of the complete scanned areas between the different plant lines and the mock- and *P. infestans*-inoculated leaves, relative quantification was performed using the manufacturer's software. The quantity is expressed in weight percentage, which is a relative concentration for the mass fraction of the chemical elements. The chemical element compositions determined for different plant types and treatments are given in Table 1. For the compatible cv. Désirée–*P. infestans* interaction, additional image analysis was performed to compare the distribution of chemical elements within the necrotic lesion area versus the green tissue area outside the necrotic lesion (Figure 4).

Local redistribution of phosphorus in infected cv. Désirée

The element maps for the macronutrient P showed a slight accumulation in the necrotic zone of the lesion in cv. Désirée (Figure 2). However, when comparing the average pixel intensity of the disease lesion area versus the area outside the disease lesion no significant differences were observed (Figure 4). For 3R no change in the P distribution was observed (Figure 2). In some of the scanned 1R leaves a faint accumulation in the HR lesion was observed; however, this was not observed in all scanned leaves. When comparing the weight percentage of P of the whole scanned areas of the three different plant lines, the inoculation with *P. infestans* did not lead to significant changes in the P content compared to the control of the same plant lines (Table 1). This indicates that the patterns observed in the element maps are due to minor local, rather than systemic, redistributions.

Depletion of potassium in necrotic tissue but an overall increase in infected cv. Désirée

In cv. Désirée, a clear depletion of the mobile macronutrient K in the necrotic zone was visible (Figure 2). Image analysis of the lesion area compared to the area outside the lesion confirmed a significantly lower pixel intensity in the lesion area compared to the area outside of the lesion (Figure 4). In both 1R and 3R, K depletion in the HR necrotic areas was also observed (Figure 2). When comparing the weight percentages of K in cv. Désirée and the two R-gene lines, we found a significantly higher percentage of K in 1R and 3R compared to cv. Désirée under control conditions (Table 1). Additionally, even though a clear depletion in the necrotic zone was observed for cv. Désirée, the overall weight percentage of K of the whole scanned area increased in the *P. infestans*-infected samples compared to uninfected samples. No significant change upon inoculation with *P. infestans* was observed for 1R and 3R.

No clear changes in sulphur distribution were observed using benchtop μXRF

In cv. Désirée a minor S accumulation was visible in the necrotic area of the lesion, but this change was not as distinct as the K depletion and the increased pixel intensity in the lesion area was not significantly higher than that in the area outside of the necrotic area (Figures 2 and 4). No significant difference in the weight percentage of S in the whole scanned area was observed in control conditions or upon inoculation with *P. infestans* (Table 1). Additionally, no redistribution of S or differences in the weight percentages were observed in 1R and 3R lines (Figure 3 and Table 1).

Distinct spatial redistribution of calcium and magnesium in the inoculated 1R line

The macronutrients Ca and Mg both showed a slight accumulation in the centre of the necrotic zone in cv. Désirée;

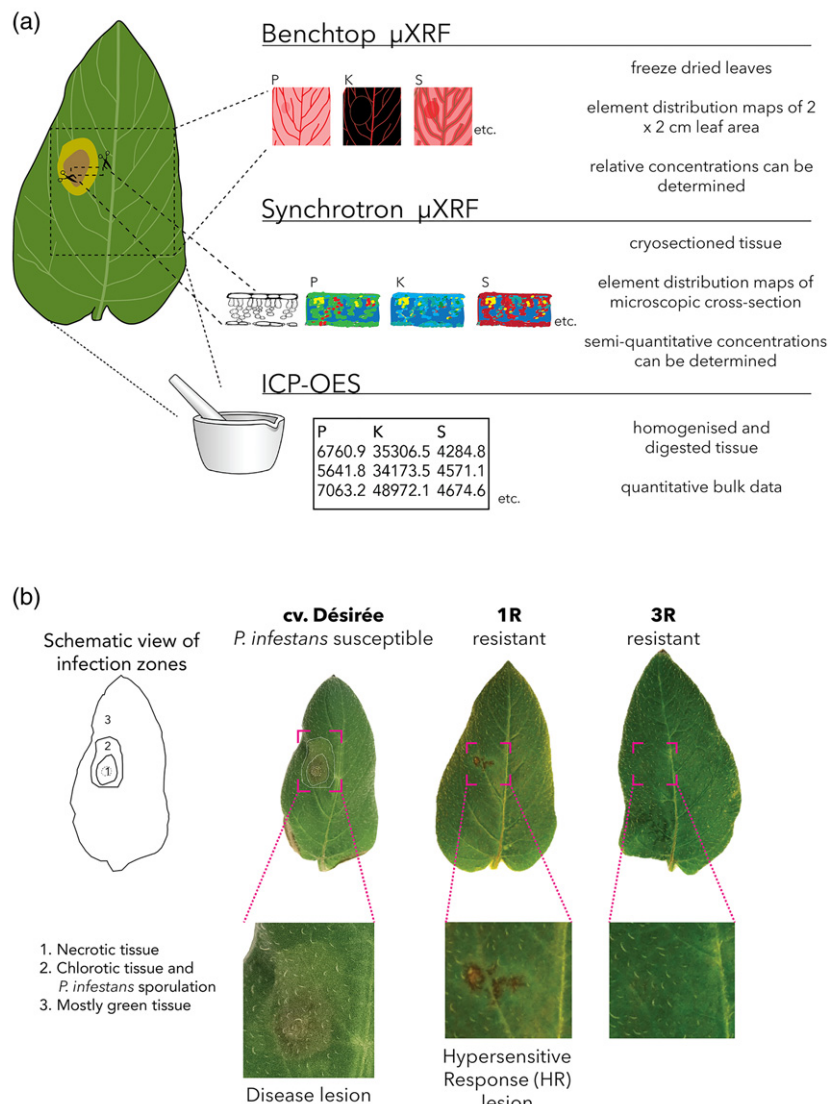


Figure 1. Overview of techniques and plant lines used in this study. (a) Summary of the different methods used to analyse elemental concentrations and distributions in potato leaves used in this paper: benchtop- and synchrotron-based micro-X-ray fluorescence (μ XRF) and inductively coupled plasma optical emission spectroscopy (ICP-OES). (b) Representative photographs of leaflets from the three plant lines 120 hpi with *Phytophthora infestans*. For the susceptible cv. Désirée, the three different infection zones within the disease lesion (adapted from van West *et al.*, 1998) are indicated with a dotted line on the photograph and in the schematic drawing next to it. Zone 1 corresponds to the necrotic tissue with the inoculation spot in the middle, zone 2 corresponds to chlorotic potato tissue and zone 3 contains green tissue.

however, these accumulation patterns did not result in significant differences in pixel intensity between the lesion and non-lesion areas (Figures 2 and 4). Yet when looking at the whole scanned area, the overall weight percentage of Mg in the *P. infestans*-infected cv. Désirée was significantly decreased compared to the control (Table 1). Clearer redistribution patterns of Ca and Mg were observed in *P. infestans*-inoculated 1R. Both elements showed an accumulation in the areas corresponding to the HR lesion and a small ring of depletion around the HR lesion (Figure 2). This redistribution, however, did not lead to significant

differences in the weight percentages of Ca and Mg between control and *P. infestans*-inoculated 1R leaves, indicating that these patterns are due to local redistribution (Table 1). In *P. infestans*-inoculated 3R leaves, a depletion area of Mg in the inoculation spot was visible, but this redistribution did not lead to significant changes in the weight percentage of Mg in the control and inoculated 3R plants (Table 1). However, overall, the weight percentage of Mg was significantly higher in both control and *P. infestans*-inoculated 3R leaves compared to the other plant lines (Table 1).

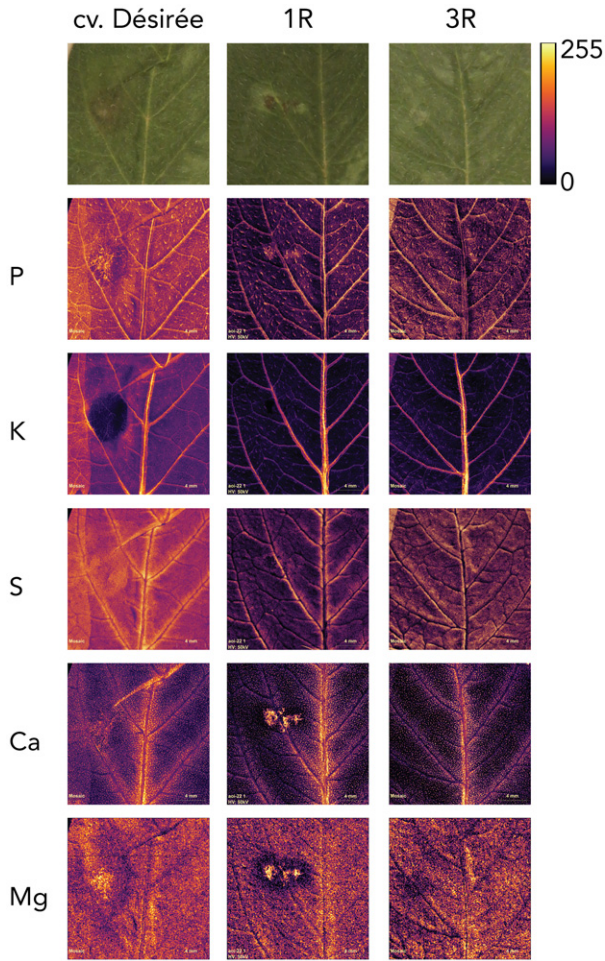


Figure 2. Element distribution maps obtained by benchtop μ XRF of macronutrients after *Phytophthora infestans* inoculation. Representative maps for phosphorus (P), potassium (K), sulphur (S), calcium (Ca) and magnesium (Mg) of freeze-dried *P. infestans*-inoculated potato leaflets at 120 hpi of three different plant lines: cv. Désirée, 1R (transgenic line containing the *Rpi-blb1* R-gene) and 3R (transgenic line containing the R-genes *Rpi-blb1*, *Rpi-blb2* and *Rpi-vnt1*). The top images show photographs of the leaflets after freeze-drying; photographs of the leaflets before freeze-drying are shown in Figure 1b.

Iron and aluminium changes observed only in the necrotic zone of susceptible interactions

The element distribution maps obtained using the benchtop μ XRF spectrometer showed no clear changes upon inoculation with *P. infestans* for the R-gene plant lines. In the susceptible cv. Désirée an accumulation or redistribution in the necrotic tissue was observed and the pixel intensity in the lesion area was significantly higher than that in the area outside the lesion (Figures 3 and 4). For Al a similar depletion pattern to that of K was observed in the disease lesion in the susceptible cv. Désirée (Figure 3). The Al pixel intensity in the necrotic area was significantly lower than outside the lesion area (Figure 4). Similar to K, we also observed a significantly higher weight percentage

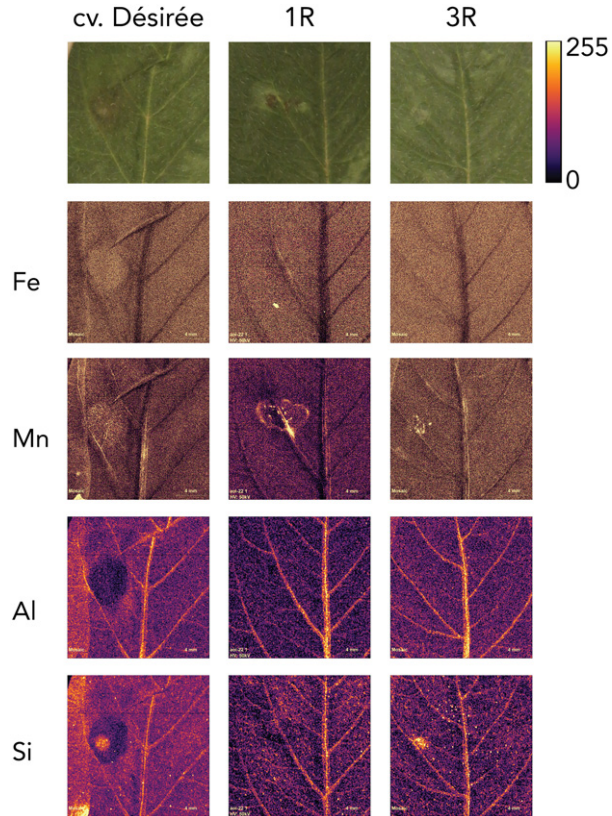


Figure 3. Element distribution maps obtained by benchtop μ XRF of micronutrients and trace elements after *Phytophthora infestans* inoculation. Representative maps for iron (Fe), manganese (Mn), aluminium (Al) and silicon (Si) of freeze-dried *P. infestans*-inoculated potato leaflets at 120 hpi of three different plant lines: cv. Désirée, 1R (transgenic line containing the *Rpi-blb1* R-gene) and 3R (transgenic line containing the R-genes *Rpi-blb1*, *Rpi-blb2* and *Rpi-vnt1*). The top images show photographs of the leaflets after freeze-drying; photographs of the leaflets before freeze-drying are shown in Figure 1b.

of Al in the 1R and 3R lines compared to cv. Désirée in control conditions (Table 1).

Immune-specific manganese and silicon spatial redistribution

For both Mn and Si, in the susceptible cv. Désirée rearrangements were observed after infection with *P. infestans*. Mn is slightly but significantly increased in the lesion area compared to the area outside the lesion (Figures 3 and 4). Si showed a depletion ring in the necrotic zone around the spot of inoculation where Si is not depleted (Figure 3). Overall, however, Si is significantly decreased in the lesion area compared to the area outside the lesion (Figure 4). Perhaps more interesting are the responses to inoculation with *P. infestans* observed in the R-gene lines. Upon *P. infestans* inoculation, in both 1R and 3R a ring of increased Mn spots was observed around the HR lesion (Figure 3). For Si no clear changes were observed in 1R. Yet, *P. infestans*-inoculated 3R showed a clear

Table 1 Elemental composition (wt. %) of the whole scanned areas of healthy and *Phytophthora infestans*-infected potato leaves as determined by benchtop μ XRF

	P	K	S	Ca	Mg	Fe	Mn	Al	Si
cv. Désirée control	13 ^A	26 ^B	5.8 ^A	11 ^{AB}	5.3 ^B	0.080 ^B	0.11 ^B	0.22 ^C	0.17 ^{AB}
cv. Désirée infected	12 ^{AB}	30 ^A	4.8 ^{AB}	12 ^A	4.2 ^C	0.090 ^{AB}	0.13 ^B	0.22 ^C	0.13 ^{ABC}
1R control	12 ^{AB}	33 ^A	5.4 ^{AB}	8.2 ^B	4.9 ^{BC}	0.086 ^{AB}	0.11 ^B	0.27 ^{AB}	0.070 ^C
1R infected	11 ^{AB}	32 ^A	4.6 ^B	11 ^{AB}	4.8 ^{BC}	0.083 ^B	0.13 ^{AB}	0.26 ^B	0.11 ^{BC}
3R control	9.2 ^{BC}	32 ^A	5.6 ^A	11 ^{AB}	6.3 ^A	0.097 ^A	0.12 ^B	0.29 ^A	0.10 ^{BC}
3R infected	8.3 ^C	30 ^A	5.3 ^{AB}	14 ^A	6.6 ^A	0.098 ^A	0.16 ^A	0.29 ^A	0.18 ^A
Coefficient of variation (%)	11	12	5.2	22	18	9.2	10	8.5	35

Weight percentages for magnesium (Mg), aluminium (Al), silicon (Si), phosphorus (P), sulphur (S), potassium (K), calcium (Ca), manganese (Mn) and iron (Fe) for cv. Désirée control ($n = 3$) and *P. infestans*-infected ($n = 4$), 1R control ($n = 3$) and *P. infestans*-infected ($n = 6$) and 3R control ($n = 3$) and *P. infestans*-infected samples ($n = 4$). All samples were harvested 120 h post-inoculation. For each element, a one-way ANOVA followed by Fisher LSD pairwise comparison with 95% confidence was performed. The letters behind the averages correspond to the Fisher LSD grouping information, where sample averages with different letters are significantly different. The mean coefficient of variation of the ANOVA is given for each element.

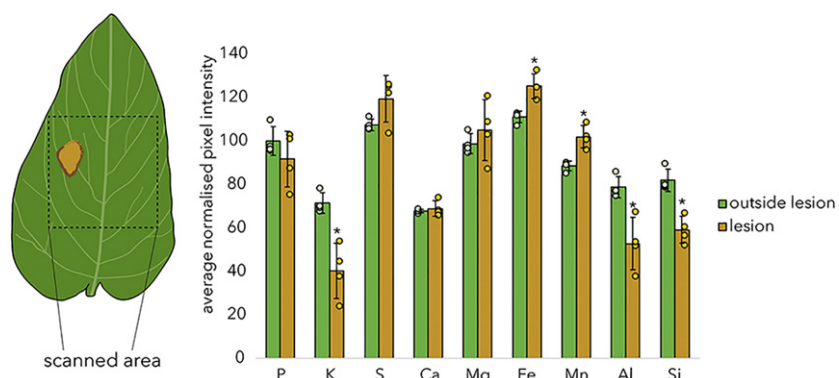


Figure 4. Average normalised pixel intensity inside the necrotic lesion area and outside the necrotic lesion in *Phytophthora infestans*-infected cv. Désirée. * $P < 0.05$ between the lesion area and outside the lesion, two-sample t-test.

accumulation of Si in the inoculation spot (Figure 3). Additionally, the Mn and Si weight percentages were significantly higher in inoculated 3R than in the control 3R leaves (Table 1). This indicates that the observed spatial changes are not due to local redistributions within the scanned area.

Synchrotron μ XRF maps reveal redistribution of elements in infected zones of cv. Désirée

We next performed synchrotron μ XRF mapping of cryosectioned samples to study the effects of *P. infestans* inoculation on the ionome with a higher resolution at the anatomical level. Element maps were obtained for all elements that were above the respective limit of detection, namely the macronutrients P, K, S and Ca and the micronutrients Fe, Mn, Zn and Cl (Figure 5 and File S2). Data on the average concentrations of elements in the samples were extracted from calibrated element maps using image analysis (Figure 5 and Table 2). For the susceptible cv. Désirée infected with *P. infestans*, samples were prepared so that both the necrotic and chlorotic zones were included. When comparing the samples from

these zones with uninfected cv. Désirée samples, several changes in elemental distribution and/or abundance were observed (Figure 5). P and S were significantly increased in both zones of infection compared to the control, with the highest concentration in the necrotic zone (Figure 5a, b). Similar to the results obtained with the benchtop μ XRF scanner, we observed that K was increased in *P. infestans*-infected samples compared to the control, with the highest concentration of K in the chlorotic zone (Figure 5a,b). For Ca there was a trend for an increased concentration in the necrotic zone. Most of the Ca appeared in idioblasts, but in the necrotic zone there appeared to be a higher amount of Ca outside of the idioblasts compared to that in the chlorotic zone or in uninfected cv. Désirée (Figure 5a,b). The micronutrients Fe, Mn, Zn and Cl all showed an increased concentration in infected samples compared to the control, with a significantly higher amount in the necrotic zone compared to the chlorotic zone, with the exception of Cl, which showed the inverse (Figure 5a,c). The element maps of the necrotic and chlorotic infection zones, in general, correspond well to the patterns observed in the element maps of freeze-

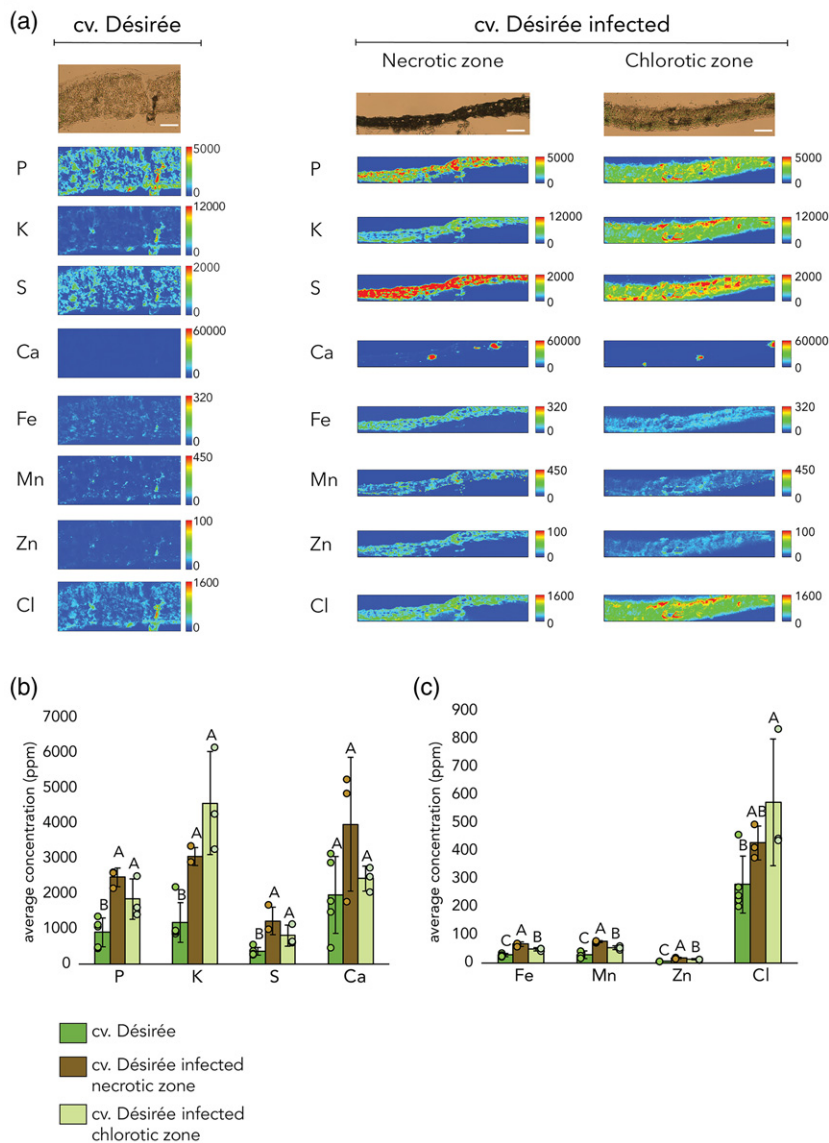


Figure 5. Element maps and element concentrations in *Phytophthora infestans*-infected and control samples obtained using semi-quantitative synchrotron μ XRF. (a) Representative element heat maps in ppm for cv. Désirée control and *P. infestans*-infected leaflets 120 hpi in the necrotic zone and the chlorotic zone. Light microscopy images of the scanned zones are displayed on top, where the size bars all correspond to 100 μ m. Synchrotron μ XRF maps obtained with a 2 μ m beam diameter at 5 keV for phosphorus (P) and sulphur (S) and 11 keV for potassium (K), calcium (Ca), manganese (Mn), iron (Fe), zinc (Zn) and chlorine (Cl). The images are presented with the adaxial side on the top. (b, c) Averages of element concentrations in ppm as determined by semi-quantitative synchrotron μ XRF for the macronutrients phosphorus (P), potassium (K), sulphur (S), calcium (Ca) (b) and the micronutrients and trace elements iron (Fe), manganese (Mn), zinc (Zn) and chlorine (Cl) (c) for cv. Désirée control ($n = 5$) and *P. infestans*-infected samples at 120 hpi in the necrotic ($n = 3$) and chlorotic zones ($n = 3$). For each element, a one-way ANOVA followed by Fisher LSD pairwise comparison with 95% confidence was performed. The error bars display the standard deviation and the letters above the error bars correspond to the Fisher LSD grouping information, where sample averages with different letters are significantly different.

dried leaves obtained using the benchtop μ XRF spectrometer (Figures 2 and 3).

Synchrotron μ XRF reveals increased average concentrations for multiple elements in susceptible interaction

All the element concentrations obtained by synchrotron μ XRF mapping were extracted from the calibrated element

maps using image analysis, and averages of the measured elements were calculated in the three different plant lines and two different treatments, mock and *P. infestans* inoculation (Table 2). The semi-quantitative concentrations of the scanned average revealed a significant increase in P, K, S, Fe, Mn, Zn and Cl in *P. infestans*-infected cv. Désirée samples compared to the control samples (Table 2). No significant differences were observed in either 1R or 3R

upon inoculation with *P. infestans*. Additionally, no significant differences were observed between the control conditions of the three different plant lines.

Exclusion of idioblasts in synchrotron μ XRF maps reveals an increase of calcium in susceptible interactions

From both the benchtop scanned maps and the synchrotron maps it is clear that Ca predominantly appears in specific areas, the idioblasts (Figures 2 and 4). Since these idioblasts do not occur evenly in the cryosectioned samples, the idioblast areas were removed from the analysis to obtain information about the level of non-idioblast Ca present in the sample (Figure 6). When excluding the idioblasts, infection with *P. infestans* led to a significant increase of Ca in cv. Désirée. For 1R and 3R no significant changes were found (Figure 6).

Absolute quantification of susceptible interaction using ICP-OES

We next aimed to obtain data on the element concentrations using a quantitative method for comparison with the μ XRF data. Therefore, ICP-OES was performed on homogenised whole leaves of both control and *P. infestans*-infected cv. Désirée leaf samples (Table 3). A significant increase in P, S and molybdenum (Mo) and a significant decrease in nickel (Ni) were observed in the *P. infestans*-infected samples compared to the control (Table 3).

DISCUSSION

In this paper, we used three different methods to visualise and quantify the changes that occur in the ionome of plant leaves with varying levels of disease susceptibility after inoculation with a plant pathogen. The methods used reveal local rearrangements of several elements in the susceptible interaction, with patterns of both accumulation and depletion observed in disease lesions. Moreover, several elements display different redistribution patterns in both or one of the resistant plant lines compared to the susceptible cultivar. The data generated demonstrate that elemental distribution can be observed in plant-pathogen interactions, with a good agreement overall between the three methods. This represents a significant technical advance in plant-microbe interactions research.

Comparison of changes in element concentrations obtained using three different methods

The benchtop μ XRF method allowed for scanning of large areas of freeze-dried leaves, and was thus capable of providing maps containing information on elemental distribution in three different zones of disease lesions at the leaf morphological level. The elemental data obtained with the benchtop μ XRF method are based on samples relatively near to the leaf surface, although the sample volume depends on the penetration depth of the ingoing X-ray, a

process that is element-, wavelength- and matrix-dependent. In comparison, the synchrotron μ XRF method allowed for scanning with a higher resolution but required thinner samples and smaller scan areas. These size restrictions are largely due to beam time limitations, since larger samples require longer scanning time. However, the higher-resolution data from the synchrotron μ XRF method allowed us to gain anatomical insights. Additionally, we used ICP-OES, a quantitative method that requires homogenised samples and is thus, in contrast to μ XRF, not able to visualise spatial redistributions within a sample. We chose control and *P. infestans*-infected cv. Désirée leaves for a comparison of the results obtained using the different methods (Table 4). It is important to note that not all the methods could be used to obtain data of all elements in the leaves. With ICP-OES we were able to obtain concentrations for more elements than with the XRF-based techniques. This was, for example, either due to limitations in sensitivity because of the low concentration of some of the trace elements or because the fluorescence excitation energy was either too low or too high to detect certain elements. Whilst the μ XRF data allowed us to pinpoint morphological or anatomical elemental differences, the element concentrations obtained from ICP-OES, on the contrary, are the average values of the elements of the whole leaf.

In Table 4 we compared the benchtop μ XRF data in weight percentages (Table 1), the semi-quantitative data in ppm obtained by synchrotron μ XRF (Table 2), and the quantitative data in ppm obtained by ICP-OES (Table 3). It is important to note that the benchtop μ XRF and ICP-OES data on *P. infestans*-infected material included parts of all three zones of infection, whereas in the synchrotron analysis only infection zones 1 and 2 were analysed. When looking at changes in the elemental distribution patterns, determined by the three different methods, after infection compared to control conditions there are no direct contradictions. For the macronutrients P and S no significant differences were observed using the benchtop μ XRF, whilst the other methods showed significant increases in these elements. It is possible that the lower resolution and lack of quantification for this method contributed to this. For Fe, Mn and Zn, a significant increase was observed using synchrotron XRF, but this was not observed using the other methods. A possible explanation for this could be the abovementioned differences in the infection zones analysed with the different methods. When just comparing zone 1 (necrotic tissue) with the rest of the tissue outside of the lesion for the benchtop μ XRF maps, a significant increase of Fe and Mn was found in the necrotic tissue (Figure 4).

In this study, we used μ XRF as a comparative tool to study elemental changes in inoculated and uninoculated tissues. However, the fluorescence data from the synchrotron XRF were converted to ppm values based on measurements of reference material obtained in a similar

Table 2 Averages of element concentrations in ppm as determined by semi-quantitative synchrotron μ XRF

	P	K	S	Ca	Fe	Mn	Zn	Cl
cv. Désirée control	910 ^B	1187 ^B	371 ^B	1970 ^{AB}	28 ^C	29 ^B	6.4 ^C	280 ^B
cv. Désirée infected	2187 ^A	4277 ^A	1019 ^A	3027 ^A	59 ^A	69 ^A	15 ^A	553 ^A
1R control	1083 ^B	1547 ^B	518 ^B	669 ^B	36 ^{BC}	31 ^B	9.1 ^{BC}	260 ^B
1R infected	781 ^B	1367 ^B	389 ^B	1314 ^B	32 ^{BC}	29 ^B	7.9 ^{BC}	226 ^B
3R control	515 ^B	1691 ^B	374 ^B	1636 ^{AB}	35 ^{BC}	41 ^{AB}	8.5 ^{BC}	369 ^{AB}
3R infected	690 ^B	1393 ^B	544 ^B	1573 ^B	43 ^B	52 ^{AB}	11 ^B	577 ^A
Coefficient of variation (%)	31	47	37	51	22	40	21	45

Concentrations (ppm) for phosphorus (P), sulphur (S), chlorine (Cl), potassium (K), calcium (Ca), manganese (Mn), iron (Fe) and zinc (Zn) for cv. Désirée control ($n = 5$) and *Phytophthora infestans*-infected ($n = 7$), 1R control ($n = 4$) and *P. infestans*-infected ($n = 4$) and 3R control ($n = 2$) and *P. infestans*-infected samples ($n = 4$). All samples were harvested at 120 h post-inoculation. For each element, a one-way ANOVA followed by Fisher LSD pairwise comparison with 95% confidence was performed. The letters behind the averages correspond to the Fisher LSD grouping information, where sample averages with different letters are significantly different. The mean coefficient of variation of the ANOVA is given for each element.

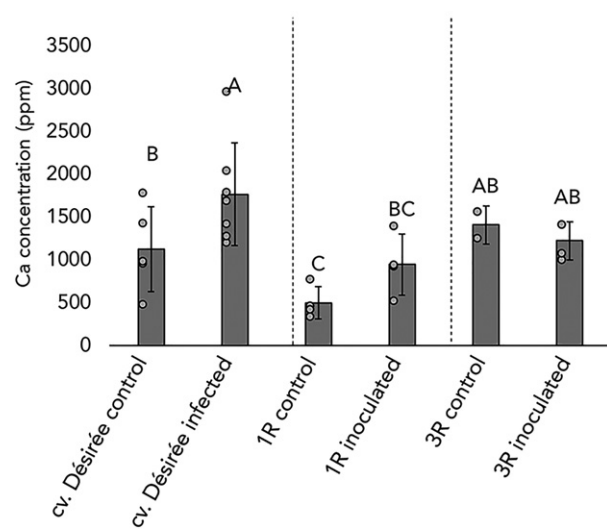


Figure 6. Calcium (Ca) concentrations, where idioblasts have been excluded. Average concentrations in ppm as detected by synchrotron μ XRF and conversion to ppm based on reference values for Désirée control ($n = 5$) and *Phytophthora infestans*-infected ($n = 7$), 1R control ($n = 4$) and *P. infestans*-infected ($n = 4$) and 3R control ($n = 2$) and *P. infestans*-inoculated samples ($n = 4$). The error bars display the standard deviation and the letters above the error bars correspond to the Fisher LSD grouping information as determined by one-way ANOVA followed by Fisher LSD pairwise comparison with 95% confidence.

fashion to the sample data. When comparing the concentrations obtained using semi-quantitative XRF with the absolute concentrations obtained using ICP-OES, there was a noticeable difference in the concentrations. The concentrations obtained with ICP-OES were on average eight times higher than those obtained using semi-quantitative analysis of the synchrotron μ XRF data. The ICP-OES elemental concentrations determined in this study were more comparable to results obtained in previous studies that looked into the influence of abiotic stress in terms of uptake of toxic elements on the elemental concentrations in potato leaves (Cao and Tibbitts, 1997; Dunbar *et al.*, 2003; Langille and

Batteese, 1974). This shows that the quantification performed using μ XRF data, which used thin-film reference material, was not as accurate for determining actual concentrations as ICP-OES. However, the μ XRF method has the advantage that it supplies spatial information and can therefore, as in this study, be used for comparative studies (Mijovilovich *et al.*, 2020; Zhao *et al.*, 2014). We conclude that the three methods are complementary to each other.

Potassium depletion in lesions and differences between plant lines

K (i.e. K^+) is a phloem-mobile macronutrient within plants and, among other things, plays a key role in the osmotic adjustment ability (Wang *et al.*, 2013). As expected, based on mobility, K was depleted in the necrotic part of the lesion compared to the area outside of the necrotic zone in all plants with a clear lesion, either a disease or HR-related lesion. However, when comparing the weight percentages of control and infected cv. Désirée obtained with benchtop μ XRF, an increase of K in the total scanned area was observed for the *P. infestans*-infected plants compared to the control (Table 1). This was also observed in the concentrations determined by synchrotron μ XRF (Table 2). Notably, no significant difference in K between control and *P. infestans*-infected cv. Désirée was observed using ICP-OES (Table 3). It is possible that this is due to the previously mentioned dilution effect from the experimental setup of the ICP-OES measurements. When comparing the weight percentages of K measured by benchtop μ XRF in the wild-type and resistant plant lines, we see a significantly lower percentage of K in cv. Désirée compared to the 1R and 3R lines under control conditions (Table 1). This result was not reproduced using synchrotron μ XRF; however, a trend for lower K in cv. Désirée samples compared to 1R and 3R under control conditions was observed (Table 2). It has been shown that K fertilisation can decrease disease severity of plants by contributing to optimal growth (Dordas, 2008). The ICP-OES measurements

Table 3 Absolute quantification of element concentrations (ppm) as measured by inductively coupled plasma optical emission spectroscopy (ICP-OES)

	P*	K	S*	Ca	Mg	Fe	Mo*	B	Cu	Mn	Na	Zn	Ni*	Co	Al	V
cv. Désirée control	5039 (1205)	49 692 (8879)	3324 (576)	17 971 (8305)	3359 (797)	194 (55)	1.0 (0.46)	31 (8.7)	6.2 (1.0)	219 (86)	94 (59)	38 (9.2)	0.42 (0.31)	0.11	10	0.015
cv. Désirée infected	6325 (2137)	47 112 (11961)	4075 (946)	13 478 (6012)	3239 (791)	203 (52)	1.7 (0.72)	30 (7.1)	8.1 (5.8)	186 (67)	75 (33)	44 (11)	0.20 (0.063)	0.10	15	0.012

Average concentrations in ppm ($\mu\text{g kg}^{-1}$ dry weight) of phosphorus (P), potassium (K), sulphur (S), calcium (Ca), magnesium (Mg), iron (Fe), molybdenum (Mo), boron (B), copper (Cu), manganese (Mn), sodium (Na), zinc (Zn), nickel (Ni), cobalt (Co), aluminium (Al) and vanadium (V) given for cv. Désirée control ($n = 20$) and *Phytophthora infestans*-infected samples ($n = 20$) at 120 h post-inoculation. The standard deviation is given in between brackets. * $P < 0.05$ between control and infected samples, two-sample t-test.

Table 4 Summary of changes in element concentration obtained using three different methods

Element	Benchtop μXRF	Synchrotron μXRF	ICP-OES
P	-	↑	↑
K	↑	↑	-
S	-	↑	↑
Ca	-	-	-
Mg	↓	x	-
Fe	-	↑	-
Mo	x	x	↑
Bo	x	x	-
Cu	x	x	-
Mn	-	↑	-
Zn	x	↑	-
Ni	x	x	↓
Cl	x	↑	x
Al	-	x	-
Si	-	x	x

Benchtop μXRF (comparative data), synchrotron μXRF (semi-quantitative data) and ICP-OES (quantitative data) were used to determine the element concentrations in cv. Désirée control and *P. infestans*-infected samples. (↑) indicates that the concentration of the element was significantly higher in infected samples compared to control. (↓) indicates that the concentration of the element was significantly lower in infected samples compared to control. (-) indicates no significant difference and (x) indicates that the element was not measured using the indicated method.

reveal a K concentration of around 5% dry weight in cv. Désirée. The optimal K level for potato yield was determined to be between 5 and 6% dry weight, with a decrease in yield when exceeding 6% (Prummel and Barnau-Sijthoff, 1984). The levels in cv. Désirée were thus not too low. The μXRF data, however, indicated a slightly higher concentration of K in the R-gene plant lines compared to cv. Désirée. In a large transcriptomic study, Alexandersson *et al.* (2020) identified effects correlated to the presence of R-genes and showed they can have an influence on gene expression even in the absence of the pathogen. One of the transcripts highly correlating with *P. infestans* leaf resistance encodes a Na/K/Ca exchanger, and several other K transporter-encoding transcripts were also correlated with *P. infestans* resistance. It is possible that the addition of R-genes in 1R and 3R leads to an increase in the expression of K transporters that influence K uptake or distribution within the plant. However, this remains to be tested.

Increased sulphur due to *P. infestans* infection in susceptible cultivar

Both the element maps obtained by synchrotron μXRF and the ICP-OES analysis revealed a significant increase of S in *P. infestans*-infected cv. Désirée. S is an essential macronutrient and is required as a component of the amino acids cysteine and methionine, as well as certain vitamins and secondary metabolites (Capaldi *et al.*, 2015). S metabolism,

by the production of glutathione, phytoalexins, glucosinolates and other S-containing secondary metabolites, is linked to the detoxification of ROS, pathogen recognition and other responses to infection (Bloem *et al.*, 2015). The increase of S observed in our study is likely due to plant responses to infection by *P. infestans*.

Calcium idioblasts and redistribution

Both μ XRF methods used in this paper elucidate the presence of Ca hotspots, the idioblasts, in which Ca is present as insoluble Ca^{2+} oxalate (Hoegen *et al.*, 2002; McNair, 1932). Ca, which is present as Ca^{2+} ions, is generally considered as the most immobile macronutrient in plants, since it is defined as phloem-immobile and has a high affinity to cell walls. Thus, it cannot be transported from old growth to new and the mobility of Ca within cells is low due to rapid chelation (Chishaki *et al.*, 2007; Tuteja and Mahajan, 2007). Nonetheless, intracellular transport of Ca is very important since Ca functions as a signalling molecule. For example, cytosolic Ca spikes are a critical part of triggering responses to abiotic and biotic stresses (Tuteja and Mahajan, 2007). Despite Ca being relatively immobile, the benchtop μ XRF maps of 1R revealed a clear increase of non-idioblast Ca in the HR lesion. Additionally, in the elemental maps obtained by synchrotron μ XRF, we observed an increase of Ca outside of the idioblast upon infection with *P. infestans* in cv. Désirée (susceptible interaction). Dixon *et al.* (1991) and Hoegen *et al.* (2002) showed that PR proteins can be targeted to and accumulate in the crystal idioblasts in tobacco and potato, respectively. Hoegen *et al.* (2002) suggested that the Ca oxalate-rich idioblasts could provide a mechanism for regulation of free Ca^{2+} and that the accumulation of PR proteins in the idioblasts indicates a role in plant defences.

Local changes in magnesium

In the benchtop μ XRF analysis, a distinct accumulation of Mg in the necrotic tissue as well as a ring of depletion corresponding to chlorotic tissues was observed in both cv. Désirée and 1R after inoculation with *P. infestans*. However, in the comparison of the pixel intensity of Mg in lesion tissue versus tissue outside the lesion and in the ICP-OES analysis between *P. infestans*-infected and uninoculated material, no significant difference in Mg was observed. This indicates the patterns observed in the maps correspond to local redistribution of Mg. Mg is an essential macronutrient and required for photosynthesis as part of the chlorophyll molecule. Mg deficiency in plants leads to chlorosis and necrosis of the leaf tissue and transport of Mg from older to younger leaves (Tanoi and Kobayashi, 2015). However, the underlying mechanisms for Mg deficiency-triggered chlorosis and remobilisation are not fully understood (Peng *et al.*, 2019). Additionally, local redistributions due to pathogen infection or immune

responses as observed in our element maps require further research.

Immune-specific spatial redistribution of manganese

The elemental maps obtained by benchtop μ XRF revealed a difference in Mn distribution after *P. infestans* inoculation in the R-gene-carrying lines compared to the susceptible cultivar. Both the 1R and 3R leaflets exhibited a halo of increased Mn around the HR lesion, and a significant increase in the weight percentage of Mn in inoculated 3R samples compared to uninoculated samples was observed. No change was observed for the Mn concentration as determined by synchrotron XRF, which could be due to the fact that only small areas were scanned. Thus, it is feasible that this increased ring did not appear within some or any of the synchrotron-scanned areas.

Mn plays a key role in several physiological processes that can be linked to disease resistance, including lignin biosynthesis and activation of the antioxidant system. In plant leaves, the minimum Mn concentration is approximately 20 ppm, whereas toxicity typically occurs above 400 ppm. Hence, our plants were well supplied with Mn, and consequently did not show any visual symptoms of deficiency/toxicity. While it is documented that Mn-deficient plants are susceptible to pathogen attack (Schmidt and Husted, 2019), the effects and roles of Mn in Mn-sufficient plants remain obscure. As a cofactor of numerous enzymes involved in lignin biosynthesis, we speculate that Mn re-allocation to lesions may be a way for the plants to reinforce infected or neighbouring cells to provide extra rigidity in an attempt to seal off the infected area.

Another Mn-related effect may be in relation to germins and germin-like proteins (GLPs). These proteins can, among other functions, facilitate the oxidation of oxalate, generating hydrogen peroxide (H_2O_2), and GLPs have been described as pathogenesis-related proteins (Pei *et al.*, 2019). Additionally, GLP overexpression and silencing studies provide evidence for a role of these proteins in resistance against several pathogens (Bernier and Berna, 2001; Pei *et al.*, 2019; Zhang *et al.*, 2018). The crystal structure of germin revealed that the protein is a homohexamer containing six Mn ions (Woo *et al.*, 2000). It is possible that the halo of Mn we observed in the R-gene-carrying lines is due to an increased abundance of proteins such as GLPs, using Mn as a cofactor, that are involved in the HR response. However, it has also been suggested that Mn could act as an antioxidant itself (Alejandro *et al.*, 2020). The previously mentioned study by Alexandersson *et al.* (2020) found several transcripts annotated as *germin* or belonging to the *germin* subfamily that correlated with *P. infestans* resistance in potato. Additionally, a recent proteomics study showed an increase in abundance of germin upon *P. infestans* inoculation in the same 1R line used in

this study (Resjö *et al.*, 2019). Interestingly, Mn has also been shown to have a direct influence on the growth of a *Phytophthora* species. Mycelial growth, sporangia production, and germination of the broad host range pathogen *Phytophthora nicotianae* were shown to be reduced by the addition of Mn (Luo *et al.*, 2020).

Immune-specific spatial redistribution of silicon

Si data in this study were only obtained using the bench-top μ XRF. When looking at the element maps, a clear accumulation spot was visible directly at the inoculation spot in the 3R line, but not in 1R, suggesting that this accumulation is not dependent on macroscopic HR or the *Rpi-blb1* R-gene but rather on one of the other R-genes. Alternatively, this Si accumulation could be an effect of the immune response triggered by multiple R-genes, independent of the exact R-genes present. Further research is required to determine how the increase in Si in the *P. infestans*-inoculated 3R line, especially at the spot of inoculation, and the resistance against *P. infestans* in this line are connected.

Si has long been known to have a positive effect on plant health and can be used to suppress a range of diseases (Wang *et al.*, 2017). The beneficial role of Si with respect to pathogen resistance could be based on the effect that Si has on cell wall integrity. As a cell wall stabiliser, Si has documented protective roles in all types of stresses, including abiotic stresses such as salinity, flooding and drought (Wang *et al.*, 2017). Interestingly, a study on the effect of Si on the infection of soybean (*Glycine max*) by the oomycete *Phytophthora sojae* found that supplying Si provided strong protection against *P. sojae*. Transcriptomics of the Si-treated and untreated plants infected with *P. sojae* revealed that the untreated plants had a high expression of defence-related genes and *P. sojae* showed high effector expression. However, in comparison, the Si-treated plants infected with *P. sojae* did not show high expression of defence-related genes and the transcriptomics seemed more similar to the uninoculated control. Additionally, the effector expression of *P. sojae* in Si-treated plants was reduced compared to the expression in untreated plants (Rasoolizadeh *et al.*, 2018). The authors hypothesise that Si interferes with the signalling network between the pathogen and plant and that this results in an incompatible interaction. This hypothesis was further developed in a review by Coskun *et al.* (2019) as the apoplastic obstruction hypothesis, in which Si depositions in the apoplast provide protection to the plant against pathogen invasion and haustorium development and thereby limit pathogen effector release, translocation to the cytoplasm and effector-receptor interactions.

Overall, the results presented in this paper show that compatible and incompatible plant-pathogen interactions lead to several elemental distribution pattern shifts. The

elements that displayed differences between the compatible and incompatible interactions present interesting targets for further elucidation of their roles in plant susceptibility and/or resistance. Future studies employing infection assays of plants fertilised with specific nutritional regimes together with detailed studies integrating ionomics with other 'omics' techniques, e.g. transcriptomics and proteomics, will enhance our understanding of resistance. Our data also indicate that the methods used here are complementary to each other.

EXPERIMENTAL PROCEDURES

Plant materials

Potato (*S. tuberosum*) plants of cultivar Désirée, referred to in the text as cv. Désirée, the transgenic line A01-22 expressing the *Rpi-blb1* R-gene in the cv. Désirée background (Abreha *et al.*, 2015), referred to in the text as 1R, and the transgenic line 3R-D1 expressing *Rpi-blb1*, *Rpi-blb2* and *Rpi-vnt1.1* in the cv. Désirée background (Wang *et al.*, 2020), referred to in the text as 3R, were maintained *in vitro* in MS20 medium (Abreha *et al.*, 2015). Fourteen-day-old *in vitro* plantlets were transferred to soil in 2-L pots containing commercial soil (Exclusiv Blom & Plantjord, Emmaljunga Torvmull AB, Sweden) supplemented with 15 ml Oscomote exact 3–4 months (16-9-12+ 2MgO +TE) fertilizer beads (ICL Speciality Fertilizers, Nordhorn, Germany). The plants were placed in an artificial light phyto-chamber with a 14-h photoperiod (160 $\mu\text{mol sec}^{-1} \text{m}^{-2}$) at 20°C and 65% relative humidity (RH) for 4 weeks. To allow acclimatisation, the plantlets were covered with a plastic cup during the first week.

Phytophthora infestans maintenance and inoculum preparation

Phytophthora infestans strain 88069 (A1 mating type, isolated in 1998 from tomato in the Netherlands) (Kamoun *et al.*, 1998; van West *et al.*, 1998) was maintained and grown on rye sucrose agar (60 g rye, 20 g sucrose and 15 g bacto agar in 1 L tap water). Fourteen-day-old cultures were flooded with cold (4°C) autoclaved tap water and placed at 4°C for 2 h to induce zoospore release as described previously (Grenville-Briggs *et al.*, 2008). The liquid was subsequently transferred through a 40- μm cell strainer and the concentration of zoospores was determined using a Fuchs Rosenthal haemocytometer. The inoculum was prepared to contain 25 000 zoospores/ml in tap water containing 0.03% bacto agar (w/v).

Plant inoculation

Plants grown in soil for 4 weeks were placed in custom-made acrylic glass boxes (422 \times 422 \times 306 mm) on a tray insert (30 mm high) containing 1 L of tap water. Each box fits four plants and when closed the RH inside the box reaches >95%. One 10- μl inoculation droplet of either *P. infestans* inoculum (25 000 zoospores/ml + 0.03% bacto agar [w/v] in tap water) or mock inoculum (0.03% bacto agar [w/v] in tap water) was added to multiple leaflets from leaves of a similar age in the middle canopy of the plant. All droplets were placed on approximately the same area of the leaflet, e.g. at a similar distance from the main vein, and not directly on a vein. The infection boxes were closed and placed in Panasonic versatile environmental test chambers (model MLR-352H-PE) equipped with 15 Panasonic FL40SS ENW/37 lights,

running the following program: 06:00–22:00, 25°C, three lights on, 90% RH; 22:00–06:00, 22°C, 0 lights on, 90% RH. For the first 24 h the lights were switched off to aid infection, and after 24 h the lids of the boxes were opened slightly. A total of 12 boxes containing four plants each were placed in four test chambers. Infected and control leaflets were harvested 120 h post-inoculation (hpi). This time point was determined after a small test experiment with *P. infestans*-infected leaves that were initially scanned using the benchtop XRF machine at 24, 48, 72 and 120 hpi. In these initial scans no alternating patterns of element distributions were detected and it was thus decided to perform all the experiments with leaf samples harvested at 120 hpi, since at this time point the different infection zones in the susceptible cultivar and clear HR lesions in the 1R line were clearly visible. Especially, for the synchrotron experiment the available beam time presented a bottle neck for the number of samples that could be imaged and thus it was decided to only use one time point after inoculation for all the experiments.

Benchtop µXRF sample preparation and measurements

Phytophthora infestans-infected and mock-inoculated potato leaflets were harvested at 120 hpi, photographed and placed in between folded printer paper. Several paper envelopes containing one leaflet each were stacked on top of each other and placed in a freeze-drying cassette consisting of two cardboard cards clasped together using two bulldog clamps. The cassette was placed at –80°C for 2 days to allow complete cooling of the tissue and was subsequently placed in a freeze dryer for 4 days. The freeze-dried leaves were photographed and placed in labelled sample bags and stored in a closed envelope at room temperature until scanning. Element distribution maps were obtained using a commercial benchtop Bruker M4 Tornado micro-energy-dispersive XRF (µ-XRF) spectrometer (Bruker Nano GmbH, Berlin, Germany). The spectrometer uses a rhodium anode X-ray tube, powered by an air-cooled high voltage generator (50 kV, 600 µA), which generates high-brilliance X-rays focused to a spot size of approximately 25 µm by polycapillary X-ray optics, while a XFlash® silicon drift detector with a 30-mm² sensitive area ensures an energy resolution of ≤145 eV for Mn K α . All measurements were carried out at 20 mbar. Several freeze-dried potato leaves were mounted next to each other on the flat surface of a Plexiglas® (polymethyl methacrylate) support resting on the sample stage. The scan area for all scanned leaves was 2.0 × 2.0 cm², centred on the inoculated zone of the inoculated leaves and the corresponding area of the control leaves. The pixel dwell time was 10 msec (15 msec for some of the measurements) and the pixel size was 10 µm, giving a total pixel number of 4.3 × 10⁶ per image. µXRF data were collected for Mg, Al, Si, P, S, K, Ca, Mn and Fe. Additional point measurements with longer exposure times of 100 msec were performed for regions that showed maximum and minimum fluorescence intensities in the element maps. These measurements showed that the fluorescence intensity is very low when an element is depleted from a region, indicating negligible concentrations of the particular element in that region, while a region showing extremely high fluorescence intensity of an element corresponds to true hotspots. M4 Tornado software from Bruker was used to calculate weight percentages based on the measured total fluorescence intensities for identified and selected elements against a calibration file. In this case we selected a calibration file based on oxides. The weight percentages were calculated over the 20 × 20-mm² scanned region. The averages presented in Table 1 are the mean of the weight percentage of the biological replicates. In total for all plant lines, element maps were obtained from three control leaves. For *P. infestans*-inoculated cv. Désirée,

1R and 3R, elemental maps were obtained from four, six and four leaves, respectively. Statistical analysis was performed using the Minitab® (Version 18) Statistical Software package (Minitab Inc., 2010). For each element, a one-way analysis of variance (ANOVA) followed by Fisher least significant difference (LSD) pairwise comparison with 95% confidence was performed.

Determining element distribution differences within scanned area. Benchtop XRF element maps of *P. infestans*-infected cv. Désirée were used to determine element distribution differences within the maps between lesion and non-lesion areas. All maps were first normalized per element in Fiji ImageJ using the process plugin Quantile Based Normalization. After normalization, the average pixel intensities of the necrotic lesion and non-lesion areas were determined for all elements and all leaves in ImageJ using the analyze measure function. To ensure selection of identical areas for all the element maps of the same leaf, selection masks were created for the lesion and non-lesion areas of each leaf. Statistical analysis was performed using the Minitab® (version 18) Statistical Software package (Minitab Inc., 2010). For each element a two-sample t-test was performed between the average pixel intensity of the lesion and non-lesion areas. The lesion and non-lesion area average pixel intensities are considered to be significantly different when $P < 0.05$.

Synchrotron µXRF sample preparation

Sections (1.5 × 0.5 cm) containing the inoculated area of potato leaflets were cut out at 120 hpi (Figure 1) and preserved in Optimum Cutting Temperature (OCT) medium (Cell Path Ltd, Newtown, UK) in a cryo mold that was quickly frozen by placing the mold on a –80°C pre-cooled solid block of Al that was placed in a Styrofoam box containing liquid N₂. Frozen samples were stored at –80°C until sectioning. The cryosectioning was performed using a cryotome (model cm1950, Leica, Germany) set to specimen and chamber temperature of –20°C. 25 µm sections were cut and loaded onto custom made Quartz slides (provided by Diamond Light Source). The samples were kept at room temperature until µXRF scanning at the Diamond Light Source. Microscopy images of the scanned areas were obtained after scanning at the Diamond Light Source using a Zeiss Axio Observer microscope (Zeiss, Germany).

Synchrotron elemental maps scanning and processing

µXRF scanning. µXRF maps were obtained with the I18 beamline at the Diamond Light Source, Didcot, UK. The samples were loaded into sample stages and oriented in such a way that the section was loaded horizontally, to limit the amount of dead space. Element maps of the samples were obtained at both 11 and 5 keV using a four-element Vortex Xspress 3 detector. The detector was positioned 50 mm from the sample and placed perpendicular to the beam path. Scanning with a pixel time of 0.1 sec was performed continuously in horizontal direction using a 2 µm × 2 µm beam. The complete sample stage was enclosed inside a helium (He) enclosure bag. The He atmosphere was released every time a new sample was placed on the sample stage. To ensure obtainment of comparable maps, the count for Si outside the sample was checked at 11 keV. If the count was approximately 80, the atmosphere in the plastic bag was satisfactory; if the count was lower, the atmosphere inside the bag was released and new He was pumped in until a satisfactory atmosphere was achieved. The obtained XRF maps were processed and quantified using the free software PyMCA (Solé *et al.*, 2007). Thin-film reference material containing seven layers of metals Ca to Mo (AXO, Dresden,

Germany) was map scanned in a similar fashion as the samples and used for quantification in PyMCA by adjusting the photon flux setting to reach the known concentrations of the reference material. These settings were subsequently used to calibrate the configuration file for fitting of all obtained elemental maps. The numbers of cryosectioned samples scanned per plant type and treatment were: cv. Désirée control $n = 5$, cv. Désirée infected $n = 7$, 1R control $n = 4$, 1R inoculated $n = 4$, 3R control $n = 2$, 3R inoculated $n = 4$.

Extraction of heat maps in PyMCA. Heat maps for all elements of all samples were extracted as PNG image files using the Matplotlib function in PyMCA. The element maps were exported as heat maps with bilinear interpolation and fixed colour scales. The minimum of the colour scale was set to 0 and the maximum was determined by calculating the median maximum value for all elements in all samples. The maximum of the colour scale was set to 5000 ppm for P, 2000 ppm for S, 1600 ppm for Cl, 12 000 ppm for K, 60 000 ppm for Ca, 450 ppm for Mn, 320 ppm for Fe and 100 ppm for Zn.

Image analysis. The mean value of the elements in ppm was determined for all samples by extracting the calibrated element maps from PyMCA as TIF files, in which the pixel values correspond to ppm, and subsequently extracting the sample pixel values in ImageJ v1.50i (Schneider *et al.*, 2012). The dead space around and inside the samples was removed for all maps of a sample by using the Si image to create a correction image. For Cl, K, Ca, Mn, Fe and Zn the 11 keV Si map was used and for P and S the 5 keV Si map was used. The new images were exported as text images and analysed in Excel. For Ca, the idioblast pixels were removed from the dataset by excluding pixel values higher than 20 000 ppm from the calculations. Statistical analysis was performed using the Minitab® (Version 18) Statistical Software package (Minitab Inc., 2010). For each element a one-way ANOVA followed by Fisher LSD pairwise comparison with 95% confidence was performed.

ICP-OES sample preparation and analysis

Phytophthora infestans-infected and mock-inoculated potato leaflets of cv. Désirée were harvested at 120 hpi. The harvested tissue was placed in 1.5-ml tubes and snap-frozen in liquid N₂. The frozen tissue was homogenised using a pre-cooled plastic pestle and subsequently freeze-dried for 48 h. Hereafter, each sample was weighed, digested using a pressurised microwave digestion system (UltraWAVE, Anton Paar GmbH, Austria) with 2.5 ml HNO₃ (70%) and 1 ml H₂O₂ (15%) and subsequently diluted to 50 ml. Elemental analysis with absolute quantification was performed with an ICP-OES (Agilent 5100, Agilent Technologies, UK), using external calibration, drift check samples and certified reference material for optimal data quality, as described in Hansen *et al.* (2013). Statistical analysis of control and infected samples was performed by two-sample *t*-test with $P < 0.05$ using the Minitab® (Version 18) Statistical Software package (Minitab Inc., 2010).

ACKNOWLEDGEMENTS

We acknowledge Diamond Light Source for time on Beamline I18 under Proposal SP24489 and support provided by the beamline scientist Tina Geraki and the mechanical technician Steve Keylock. We would like to thank Myung Ho Kook, Mayank Jain and Henrik Olesen at Nutech, DTU, Denmark for valuable discussions and Nutech, DTU for allowing the use of the M4 Tornado XRF instrument. We thank Thomas H. Hansen and Lena Byrgesson for technical expertise regarding the ICP-OES analyses. The Lund

University Bioimaging Centre (LBIC), Lund University, is gratefully acknowledged for providing experimental resources and we thank Susanne Strömblad for the cryotome training. Additionally, we would like to thank Erland Liljeroth for supervision support and critical reading of the manuscript. This work was funded by Stiftelsen Lantbruksforskning (R-19-25-282 to EA), the Swedish Foundation for Strategic Research (FFL5, Future Research Leaders Fellowship to LGB), the DFF project 'Silicon-boosting the natural stress tolerance of plants' (case nr. 9041-00022A) and FORMAS (grants 2015-00430 and 2019-00881 to LGB and grants 2015-00442 and 2020-01211 to EA).

CONFLICT OF INTEREST

The authors declare to have no conflict of interest.

SUPPORTING INFORMATION

Additional Supporting Information may be found in the online version of this article.

File S1. All element maps obtained with benchtop μ XRF.

File S2. All element maps obtained with synchrotron μ XRF.

REFERENCES

- Abreha, K.B., Alexandersson, E., Vossen, J.H., Anderson, P. & Andreasson, E. (2015) Inoculation of transgenic resistant potato by *Phytophthora infestans* affects host plant choice of a generalist moth. *PLoS One*, **10**, e0129815. <https://doi.org/10.1371/journal.pone.0129815>
- Alejandro, S., Höller, S., Meier, B. & Peiter, E. (2020) Manganese in plants: from acquisition to subcellular allocation. *Frontiers in Plant Science*, **11**, 300. <https://doi.org/10.3389/fpls.2020.00300>
- Alexandersson, E., Kushwaha, S., Subedi, A., Weighill, D., Climer, S., Jacobson, D. *et al.* (2020) Linking crop traits to transcriptome differences in a progeny population of tetraploid potato. *BMC Plant Biology*, **20**, 120. <https://doi.org/10.1186/s12870-020-2305-x>
- Amtrmann, A., Troufflard, S. & Armengaud, P. (2008) The effect of potassium nutrition on pest and disease resistance in plants. *Physiologia Plantarum*, **133**, 682–691. <https://doi.org/10.1111/j.1399-3054.2008.01075.x>
- Bernier, F. & Berna, A. (2001) Germins and germin-like proteins: plant do-all proteins. But what do they do exactly? *Plant Physiology and Biochemistry*, **39**, 545–554. [https://doi.org/10.1016/S0981-9428\(01\)01285-2](https://doi.org/10.1016/S0981-9428(01)01285-2)
- Bloem, E., Haneklaus, S. & Schnug, E. (2015) Milestones in plant sulfur research on sulfur-induced-resistance (SIR) in Europe. *Frontiers in Plant Science*, **5**, 779. <https://doi.org/10.3389/fpls.2014.00779>
- Cao, W. & Tibbitts, T.W. (1997) Starch concentration and impact on specific leaf weight and element concentrations in potato leaves under varied carbon dioxide and temperature. *Journal of Plant Nutrition*, **20**, 871–881. <https://doi.org/10.1080/01904169709365302>
- Capaldi, F.R., Gratao, P.L., Reis, A.R., Lima, L.W. & Azevedo, R.A. (2015) Sulfur metabolism and stress defense responses in plants. *Tropical Plant Biology*, **8**, 60–73. <https://doi.org/10.1007/s12042-015-9152-1>
- Caruso, F., Mantellato, S., Palacios, M. & Flatt, R.J. (2017) ICP-OES method for the characterization of cement pore solutions and their modification by polycarboxylate-based superplasticizers. *Cement and Concrete Research*, **91**, 52–60. <https://doi.org/10.1016/j.cemconres.2016.10.007>
- Champouret, N., Bouwmeester, K., Rietman, H., van der Lee, T., Maliepaard, C., Heupink, A. *et al.* (2009) *Phytophthora infestans* isolates lacking class I ipiO variants are virulent on Rpi-blb1 potato. *Molecular Plant-Microbe Interactions*, **22**, 1535–1545. <https://doi.org/10.1094/MPMI-22-12-1535>
- Chishaki, N., Yuda, K. & Inanaga, S. (2007) Differences in mobility of calcium applied to the aboveground parts of broad bean plants (*Vicia faba* L.). *Soil Science and Plant Nutrition*, **53**, 286–288. <https://doi.org/10.1111/j.1747-0765.2007.00147.x>
- Coskun, D., Deshmukh, R., Sonah, H., Menzies, J.G., Reynolds, O., Ma, J.F. *et al.* (2019) The controversies of silicon's role in plant biology. *New Phytologist*, **221**, 67–85. <https://doi.org/10.1111/nph.15343>
- De La Fuente, L., Parker, J.K., Oliver, J.E., Granger, S., Brannen, P.M., van Santen, E. *et al.* (2013) The bacterial pathogen *Xylella fastidiosa* affects

- the leaf ionome of plant hosts during infection. *PLoS One*, **8**, e62945. <https://doi.org/10.1371/journal.pone.0062945>
- Dixon, D.C., Cutt, J.R. & Klessig, D.F.** (1991) Differential targeting of the tobacco PR-1 pathogenesis-related proteins to the extracellular space and vacuoles of crystal idioblasts. *The EMBO Journal*, **10**, 1317–1324. <https://doi.org/10.1002/j.1460-2075.1991.tb07650.x>
- Dordas, C.** (2008) Role of nutrients in controlling plant diseases in sustainable agriculture. A review. *Agronomy for Sustainable Development*, **28**, 33–46. <https://doi.org/10.1051/agro:2007051>
- Dunbar, K.R., McLaughlin, M.J. & Reid, R.J.** (2003) The uptake and partitioning of cadmium in two cultivars of potato (*Solanum tuberosum* L.). *Journal of Experimental Botany*, **54**, 349–354. <https://doi.org/10.1093/jxb/erg016>
- Eriksson, D., Carlson-Nilsson, U., Ortiz, R. & Andreasson, E.** (2016) Overview and breeding strategies of table potato production in Sweden and the Fennoscandian region. *Potato Research*, **59**, 279–294. <https://doi.org/10.1007/s11540-016-9328-6>
- Foster, S.J., Park, T.-H., Pel, M., Brigneti, G., Sliwka, J., Jagger, L. et al.** (2009) Rpi-vnt1.1, a Tm-2(2) homolog from *Solanum venturii*, confers resistance to potato late blight. *Molecular Plant-Microbe Interactions*, **22**, 589–600. <https://doi.org/10.1094/MPMI-22-5-0589>
- Fry, W.** (2008) *Phytophthora infestans*: the plant (and R gene) destroyer. *Molecular Plant Pathology*, **9**, 385–402. <https://doi.org/10.1111/j.1364-3703.2007.00465.x>
- Ghislain, M., Byarugaba, A.A., Magembe, E., Njoroge, A., Rivera, C., Román, M.L. et al.** (2019) Stacking three late blight resistance genes from wild species directly into African highland potato varieties confers complete field resistance to local blight races. *Plant Biotechnology Journal*, **17**, 1119–1129. <https://doi.org/10.1111/pbi.13042>
- Grenville-Briggs, L.J., Anderson, V.L., Fugelstad, J., Avrova, A.O., Bouzenzana, J., Williams, A. et al.** (2008) Cellulose synthesis in *Phytophthora infestans* is required for normal appressorium formation and successful infection of potato. *Plant Cell*, **20**, 720–738. <https://doi.org/10.1105/tpc.107.052043>
- Graham, R.D. & Webb, M.J.** (2018) Micronutrients and disease resistance and tolerance in plants. In: Mortvedt, J. (Ed.) *Micronutrients in agriculture*. John Wiley & Sons, Ltd, pp. 329–370. <https://onlinelibrary.wiley.com/doi/abs/10.2136/sssabookser4.2ed.c10>
- Hansen, T.H., de Bang, T.C., Laursen, K.H., Pedas, P., Husted, S. & Schjoerring, J.K.** (2013) Multielement plant tissue analysis using ICP spectrometry. *Methods in Molecular Biology*, **953**, 121–141. https://doi.org/10.1007/978-1-62703-152-3_8
- Hoegen, E., Strömborg, A., Pihlgren, U. & Kombrink, E.** (2002) Primary structure and tissue-specific expression of the pathogenesis-related protein PR-1b in potato[†]. *Molecular Plant Pathology*, **3**, 329–345. <https://doi.org/10.1046/j.1364-3703.2002.00126.x>
- Jenkins, P.D. & Ali, H.** (2000) Phosphate supply and progeny tuber numbers in potato crops. *Annals of Applied Biology*, **136**, 41–46. <https://doi.org/10.1111/j.1744-7348.2000.tb00007.x>
- Jones, J.D.G. & Dangl, J.L.** (2006) The plant immune system. *Nature*, **444**, 323–329. <https://doi.org/10.1038/nature05286>
- Kamoun, S., van West, P., Vleeshouwers, V.G.A.A., de Groot, K.E. & Govers, F.** (1998) Resistance of *Nicotiana benthamiana* to *Phytophthora infestans* is mediated by the recognition of the elicitor protein INF1. *The Plant Cell*, **10**, 1413–1425. <https://doi.org/10.1105/tpc.10.9.1413>
- Kieu, N.P., Aznar, A., Segond, D., Rigault, M., Simond-Côté, E., Kunz, C. et al.** (2012) Iron deficiency affects plant defence responses and confers resistance to *Dickeya dadantii* and *Botrytis cinerea*: plant iron deficiency and resistance to pathogens. *Molecular Plant Pathology*, **13**, 816–827. <https://doi.org/10.1111/j.1364-3703.2012.00790.x>
- Langille, A.R. & Batteese, R.I.** (1974) Influence of zinc concentration in nutrient solution on growth and elemental content of the "Katahdin" potato plant. *American Potato Journal*, **51**, 345–354. <https://doi.org/10.1007/BF02852080>
- Luo, Y., Yao, A., Tan, M., Li, Z., Qing, L. & Yang, S.** (2020) Effects of manganese and zinc on the growth process of *Phytophthora nicotianae* and the possible inhibitory mechanisms. *PeerJ*, **8**, e8613. <https://doi.org/10.7717/peerj.8613>
- McNair, J.B.** (1932) The interrelation between substances in plants: essential oils and resins, cyanogen and oxalate. *American Journal of Botany*, **19**, 255–272. <https://doi.org/10.2307/2436337>
- Meyer-Aurich, A., Weersink, A., Gandorfer, M. & Wagner, P.** (2010) Optimal site-specific fertilization and harvesting strategies with respect to crop yield and quality response to nitrogen. *Agricultural Systems*, **103**, 478–485. <https://doi.org/10.1016/j.agsy.2010.05.001>
- Mijovilovich, A., Morina, F., Bokhari, S.N., Wolff, T. & Küpper, H.** (2020) Analysis of trace metal distribution in plants with lab-based microscopic X-ray fluorescence imaging. *Plant Methods*, **16**, 82. <https://doi.org/10.1186/s13007-020-00621-5>
- Nicolas, O., Charles, M.T., Jenni, S., Toussaint, V., Parent, S.É. & Beaulieu, C.** (2019) The ionomics of lettuce infected by *Xanthomonas campestris* pv. *vitiensis*. *Frontiers in Plant Science*, **10**, 351. <https://doi.org/10.3389/fpls.2019.00351>
- Pei, Y., Li, X., Zhu, Y., Ge, X., Sun, Y., Liu, N. et al.** (2019) GhABP19, a novel germin-like protein from *Gossypium hirsutum*, plays an important role in the regulation of resistance to verticillium and fusarium wilt pathogens. *Frontiers in Plant Science*, **10**, 583. <https://doi.org/10.3389/fpls.2019.00583>
- Peng, Y.Y., Liao, L.L., Liu, S., Nie, M.M., Li, J., Zhang, L.D. et al.** (2019) Magnesium deficiency triggers SGR-mediated chlorophyll degradation for magnesium remobilization. *Plant Physiology*, **181**, 262–275. <https://doi.org/10.1104/pp.19.00610>
- Prummel, J. & Barnau-Sijthoff, P.** (1984) Optimum phosphate and potassium levels in potato tops. *Fertilizer Research*, **5**, 203–211. <https://doi.org/10.1007/BF01052717>
- Rasoolizadeh, A., Labbé, C., Sonah, H., Deshmukh, R.K., Belzile, F., Menzies, J.G. et al.** (2018) Silicon protects soybean plants against *Phytophthora sojae* by interfering with effector-receptor expression. *BMC Plant Biology*, **18**, 97. <https://doi.org/10.1186/s12870-018-1312-7>
- Resjö, S., Zahid, M.A., Burra, D.D., Lenman, M., Levander, F. & Andreasson, E.** (2019) Proteomics of PTI and two ETI immune reactions in potato leaves. *International Journal of Molecular Sciences*, **20**, 4726. <https://doi.org/10.3390/ijms20194726>
- Salt, D.E., Baxter, I. & Lahner, B.** (2008) Ionomics and the study of the plant ionome. *Annual Review of Plant Biology*, **59**, 709–733. <https://doi.org/10.1146/annurev.arplant.59.032607.092942>
- Schmidt, S.B. & Husted, S.** (2019) The biochemical properties of manganese in plants. *Plants (Basel)*, **8**, 381. <https://doi.org/10.3390/plants8100381>
- Schneider, C.A., Rasband, W.S. & Eliceiri, K.W.** (2012) NIH image to ImageJ: 25 years of image analysis. *Nature Methods*, **9**, 671–675. <https://doi.org/10.1038/nmeth.2089>
- Shackley, M.S.** (2018) X-ray fluorescence spectrometry (XRF). In: Lopez Varela, S.L. (Ed.) *The encyclopedia of archaeological sciences*. American Cancer Society, pp. 1–5. <https://onlinelibrary.wiley.com/doi/abs/10.1002/9781119188230.saseas0620>
- Solé, V.A., Papillon, E., Cotte, M., Walter, P.h. & Susini, J.** (2007) A multi-platform code for the analysis of energy-dispersive X-ray fluorescence spectra. *Spectrochimica Acta Part B: Atomic Spectroscopy*, **62**, 63–68. <https://doi.org/10.1016/j.sab.2006.12.002>
- Song, J., Braeden, J.M., Naess, S.K., Raasch, J.A., Wielgus, S.M., Haberlach, G.T. et al.** (2003) Gene RB cloned from *Solanum bulbocastanum* confers broad spectrum resistance to potato late blight. *Proceedings of the National Academy of Sciences*, **100**, 9128–9133. <https://doi.org/10.1073/pnas.1533501100>
- Tanoi, K. & Kobayashi, N.I.** (2015) Leaf senescence by magnesium deficiency. *Plants (Basel)*, **4**, 756–772. <https://doi.org/10.3390/plants4040756>
- Tuteja, N. & Mahajan, S.** (2007) Calcium signaling network in plants: an overview. *Plant Signaling & Behavior*, **2**, 79–85. <https://doi.org/10.4161/psb.2.2.4176>
- van der Vossen, E.A.G., Gros, J., Sikkema, A., Muskens, M., Wouters, D., Wolters, P. et al.** (2005) The Rpi-blb2 gene from *Solanum bulbocastanum* is an Mi-1 gene homolog conferring broad-spectrum late blight resistance in potato. *The Plant Journal*, **44**, 208–222. <https://doi.org/10.1111/j.1365-313X.2005.02527.x>
- van der Vossen, E., Sikkema, A., Lintel Hekkert, B.T., Gros, J., Stevens, P., Muskens, M. et al.** (2003) An ancient R gene from the wild potato species *Solanum bulbocastanum* confers broad-spectrum resistance to *Phytophthora infestans* in cultivated potato and tomato. *The Plant Journal*, **36**, 867–882. <https://doi.org/10.1046/j.1365-313X.2003.01934.x>
- van West, P., de Jong, A.J., Judelson, H.S., Emons, A.M.C. & Govers, F.** (1998) The ipiO gene of *Phytophthora infestans* is highly expressed in invading hyphae during infection. *Fungal Genetics and Biology*, **23**, 126–138. <https://doi.org/10.1006/fgb.1998.1036>

- Wang, E.S., Kieu, N.P., Lenman, M. & Andreasson, E.** (2020) Tissue culture and refreshment techniques for improvement of transformation in local tetraploid and diploid potato with late blight resistance as an example. *Plants*, **9**, 695. <https://doi.org/10.3390/plants9060695>
- Wang, M., Gao, L., Dong, S., Sun, Y., Shen, Q. & Guo, S.** (2017) Role of silicon on plant-pathogen interactions. *Frontiers in Plant Science*, **8**, 701. <https://doi.org/10.3389/fpls.2017.00701>
- Wang, M., Zheng, Q., Shen, Q. & Guo, S.** (2013) The critical role of potassium in plant stress response. *International Journal of Molecular Sciences*, **14**, 7370–7390. <https://doi.org/10.3390/ijms14047370>
- Wang, Y., Tyler, B.M. & Wang, Y.** (2019) Defense and counterdefense during plant-pathogenic oomycete infection. *Annual Review of Microbiology*, **73**, 667–696. <https://doi.org/10.1146/annurev-micro-020518-120022>
- Westermann, D.T.** (2005) Nutritional requirements of potatoes. *American Journal of Potato Research*, **82**, 301–307. <https://doi.org/10.1007/BF02871960>
- Woo, E.-J., Dunwell, J.M., Goodenough, P.W., Marvier, A.C. & Pickersgill, R.W.** (2000) Germin is a manganese containing homohexameric oxalate oxidase and superoxide dismutase activities. *Nature Structural Biology*, **7**, 1036–1040. <https://doi.org/10.1038/80954>
- Yousef, M., Li, J., Lu, J., Ren, T., Cong, R., Fahad, S. et al.** (2017) Effects of fertilization on crop production and nutrient-supplying capacity under rice-oilseed rape rotation system. *Scientific Reports*, **7**, 1270. <https://doi.org/10.1038/s41598-017-01412-0>
- Zhang, Y., Wang, X., Chang, X., Sun, M., Zhang, Y., Li, W. et al.** (2018) Over-expression of germin-like protein GmGLP10 enhances resistance to Sclerotinia sclerotiorum in transgenic tobacco. *Biochemical and Biophysical Research Communications*, **497**, 160–166. <https://doi.org/10.1016/j.bbrc.2018.02.046>
- Zhao, F.-J., Moore, K.L., Lombi, E. & Zhu, Y.-G.** (2014) Imaging element distribution and speciation in plant cells. *Trends in Plant Science*, **19**, 183–192. <https://doi.org/10.1016/j.tplants.2013.12.001>
- Zhu, S., Li, Y., Vossen, J.H., Visser, R.G.F. & Jacobsen, E.** (2012) Functional stacking of three resistance genes against *Phytophthora infestans* in potato. *Transgenic Research*, **21**, 89–99. <https://doi.org/10.1007/s11248-011-9510-1>